Architecture and performance of the ESPER-2 hard-disk drive servo writer

The servo writer is known as the most accurate and sensitive tool on an HDD (harddisk drive) manufacturing line. ESPER-2 is designed as a product-independent common servo writer which incorporates major advances in equipment cost, reduction of clean-room requirements, and writing accuracy. The servo writing process consists of two stages. The first stage writes the master servo pattern on as many as ten disks at once with little need for contaminant protection facilities. One such master disk is then assembled with other, raw, disks in a file, and the second stage writes the proper servo pattern on all disk surfaces by referring to the master. The effects of off-center discursions in the mechanical disk assembly and random runout (NRRO, or nonrepeatable runout) in the product spindle components are eliminated by table-lookup servo actuator control, so that writing accuracy is improved. Neither an exceptionally clean environment nor fine mechanical parts are required for the secondstage operation.

Introduction

Larger capacity and higher performance are being required of all hard file products including low-end HDD (hard disk drives). To obtain faster and more accurate head position control, closed-loop servo control is generally more effective than other methods. However, servo writers are required to write fine servo patterns on the disk surfaces during manufacturing [1]. Because conventional servo writers are extremely expensive and sensitive to vibration, contamination, and electromagnetic interference, they must be operated on heavy granite anti-vibration tables in a clean room that is itself protected from vibration and shock. For high-volume production, these requirements present a considerable problem of cost and quality control. In addition, the influence on writing accuracy of NRRO (nonrepeatable runout) in components of the spindle motor cannot be compensated. This is one of the major concerns in manufacturing low-cost HDD, in which air bearings cannot be used because of their cost. ESPER (Economical Servo Pattern EmbeddeR [2]) was developed to allow office-environment operation without clean-room or antivibration facilities. However, ESPER was specially designed for compact HDDs, which have a spindle motor with an outer rotor and a rotary actuator with an extended

[®]Copyright 1993 by International Business Machines Corporation. Copying in printed form for private use is permitted without payment of royalty provided that (1) each reproduction is done without alteration and (2) the *Journal* reference and IBM copyright notice are included on the first page. The title and abstract, but no other portions, of this paper may be copied or distributed royalty free without further permission by computer-based and other information-service systems. Permission to *republish* any other portion of this paper must be obtained from the Editor.



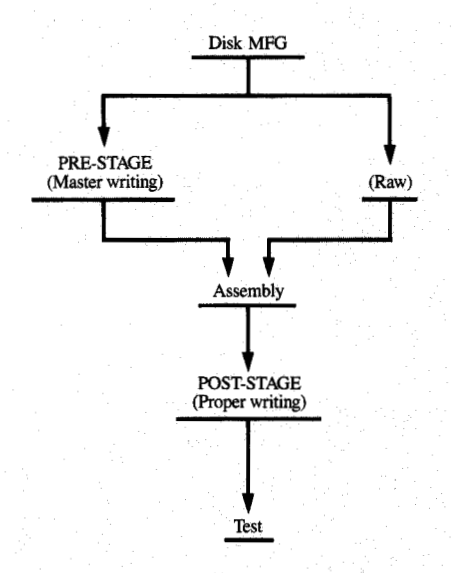


Figure 1 Servo writing process on ESPER-2 architecture.

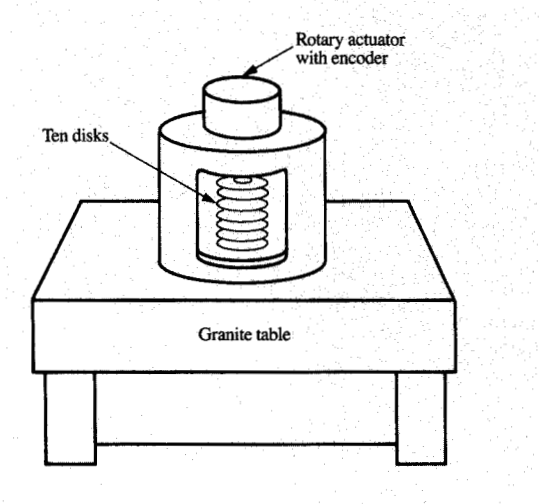
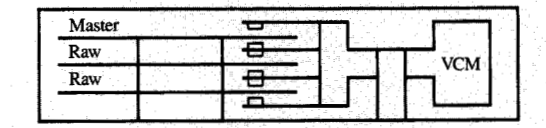


Figure 2 Pre-writer apparatus.

pivot shaft. The outer rotor is not used in more advanced low-end HDD products, in which a dual-supported in-hub motor (a spindle motor in which the rotor and stator are packed inside the hub) is used to keep mechanical resonance high. In larger file products, a linear actuator is used rather



Manning.

Disk mount at file assembly (master disk assembled with raw disks in a file).

than a rotor, and the NRRO problem has also not yet been solved in ESPER. For these reasons, the original ESPER architecture may not be practical for future products.

ESPER-2 is designed with a new architecture, which is independent of product specifications and reflects advances in total operation cost, process performance, and writing accuracy with respect to spindle NRRO.

The ESPER-2 concept

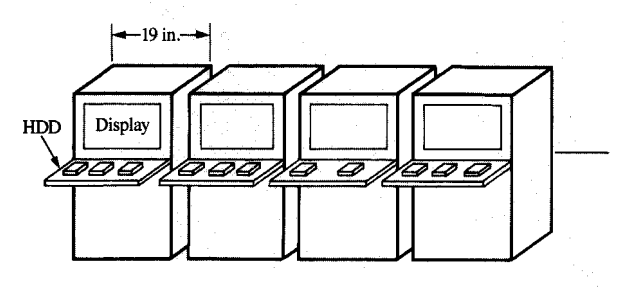
■ Dual-stage writing

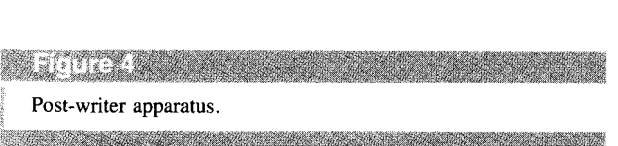
In the ESPER-2 architecture, the servo writing process is divided into two stages, as shown in **Figure 1**.

The first stage, or "pre-stage," writes the master servo pattern at the single-disk level. Figure 2 shows the pre-writer apparatus. Up to ten disks are stacked and written at once on the writer spindle. The master tracks are very precisely written in regular circles concentric with the center of the master spindle. This stage is operated in a class-100 clean environment.

One master disk is then mounted with other, raw, disks in a file, as shown in **Figure 3**. There is an offset of several tenths of a micrometer between the center of the master track circle and the center of spindle revolution in the file. The offset is fixed and stable; it is considered to be an RRO (repeatable runout) component of the master servo track.

Figure 4 shows the post-writer (second-stage) apparatus. Both head-position control and the read/write operation are electrically performed, with no fine mechanical parts. A DSP (digital signal processor) used as a digital servo actuator controller provides fast and accurate head positioning by sampling the master pattern. Disk/spindle RRO components are digitally measured and canceled by a table-lookup method. Then the post-writer writes the final (proper) servo tracks following concentric circles centered on the spindle rotation. The read/write clock is generated to be synchronous with the master pattern sector signal. The influence of RRO components on clock stability is also canceled by another table-lookup method. Finally, the





master servo pattern is erased during the product-test

process after proper servo writing is completed.

• Master and proper servo patterns

Figure 5 shows both the master and the proper servo patterns. The master pattern has several times more sectors than the proper pattern in order to provide higher sampling frequency.

Figure 6 shows examples of the master and proper servo signals. The identification part of the master signal is different from that of the proper signal, so that the master pattern can be read as a normal datum through the read/write channel of the product file, making it easy to erase.

Figure 7 shows a radial cross section of the master and proper tracks. The master tracks are written from the outer track to the inner track over nearly the entire disk surface. The position of the outer crash stop in the product file, however, is at least $1000~\mu m$ away from the edge of the disk for safety. Therefore, the master pattern can be read from any position at which the product head happens to park. The first proper track position is then determined from the crash stop using an offset from the first master track.

Pre-writer

Configuration

Figure 8 shows the pre-writer configuration. To prevent external vibration, a granite table is used for the fixture base. Air-bearing spindles are used to obtain accurate and stable disk revolution. A dc brushless motor is directly mounted in the spindle. An optical sensor is also mounted in the spindle, to accurately detect disk revolution. Nonrepeatable jitter components of the optical sensor itself must be strictly controlled to obtain a clear master pattern. Repeatable jitter components can be canceled by a PLL

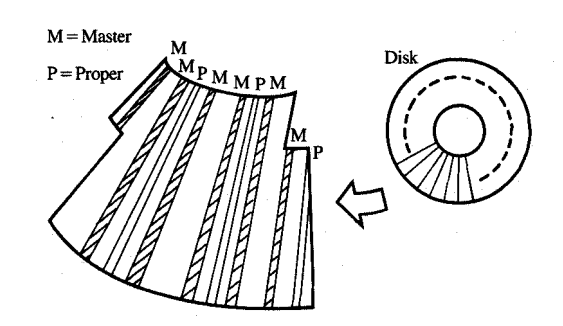


Figure 5
Allocation of master and proper sectors.

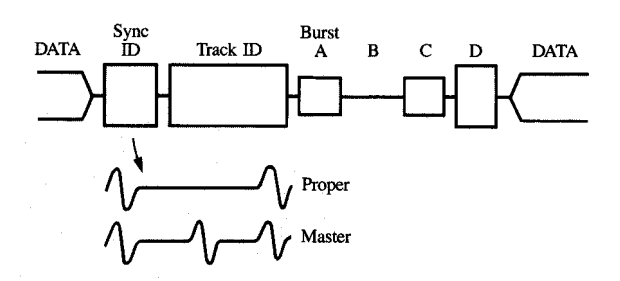


Figure 6

Master and proper servo signal example.

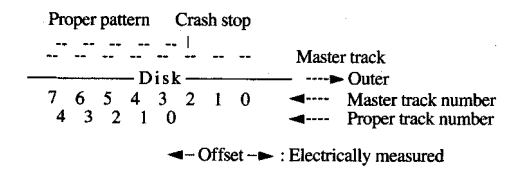
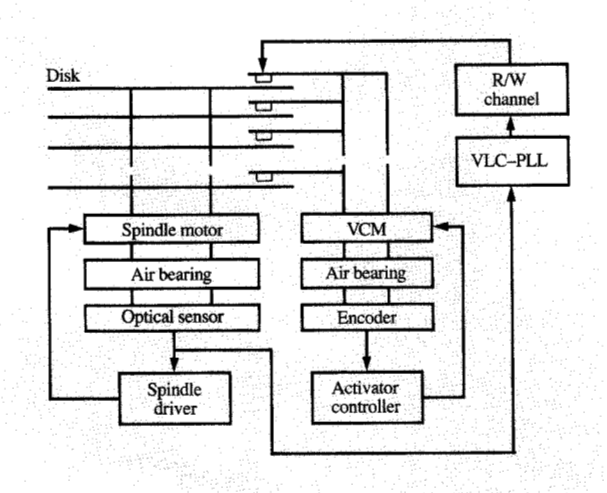
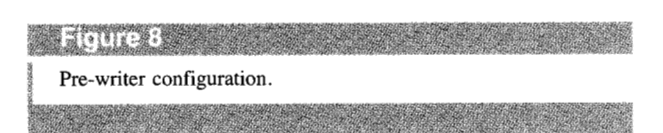


Figure 7 Radial cross section of master and proper tracks.

(phase-locked loop) circuit, as discussed later in this paper. This technique allows us to use a commercial optical encoder without special fabrication.





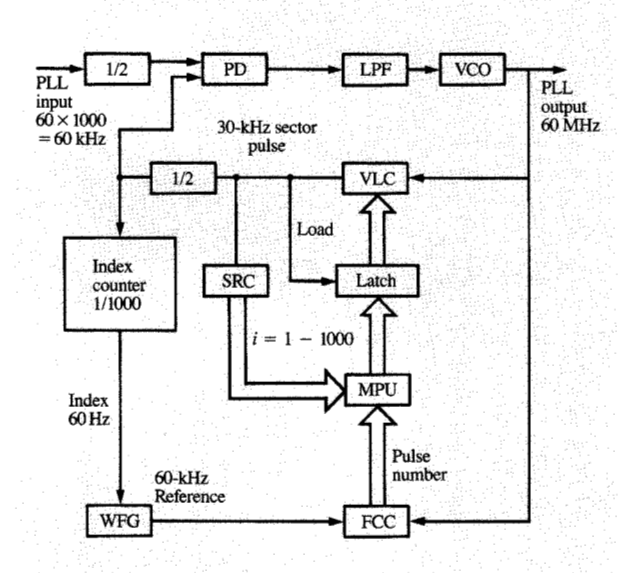


Figure 9
VLC-PLL block diagram.

An air-bearing spindle is also used to support the rotary actuator axis. A rotary dc motor is directly mounted in the air spindle. The angle of the actuator is detected by the same laser encoder technology as that used in the original ESPER actuator control system [3]. The optical pattern disk of the encoder is directly coupled with the air-bearing axis. The servo controller detects the actuator angle by canceling the encoder error and drives the dc motor directly with a current source.

The position of the first master track is initialized to a zero-reference position, such as the crash stop on the pre-writer. To write the master pattern from outer track to inner track, the position of the zero-reference position is finely tuned off-line. Tilting components of the disk spindle and actuator axis are also controlled accurately. The actuator length and its position against the disk spindle are set to be the same as the product dimensions, which reduces the difference between the pre-stage write-head yaw angle and that of the product head. The pre-writer head width is then determined to be a little wider than the product track pitch, to obtain a master-track pitch that depends on actuator control accuracy but is independent of the head width.

• Actuator control

The encoder error-cancellation algorithm is the same as that of ESPER. The actuator angle is detected to 0.04 seconds of resolution, which corresponds to about 0.01 μm of the typical 3.5-inch product-head travel range. The DSP is applied to compute the error-cancellation algorithm and the feedback flow. This approach, and a stiff actuator which has very high mechanical resonance, permit highgain servo control with a high sampling rate. The airbearing axis is much smoother than any ball-bearing assembly which has nonlinear dynamics. The applied ADC (analog-to-digital converter) and DAC (digital-to-analog converter) have enough resolution to eliminate quantization error.

• Read/write timing control

Servo read/write operations require a stable system clock that is synchronous with real motor revolution, eliminating any optical-sensor error. In ESPER architecture, the twin-PLL error canceler was developed. The following method reduces the jitter problem better than ESPER. The optical pattern disk has uniform errors, which cause repeatable jitter on the optical sensor output. A VLC-PLL (variable loop counter PLL), which is shown in Figure 9, eliminates the repeatable jitter and generates a stable system clock which is synchronous with the spindle revolution.

In Figure 9, a PD (phase detector), an LPF (low-pass filter), a VCO (voltage-controlled oscillator), and a VLC make up the PLL synthesizer. Input is the optical sensor signal. Output is the system clock. The pole of the LPF is placed to reduce high-frequency sensor error. The MPU (microprocessor unit) stores a VLC counter value for each sector. When the counter value is set to correspond to the characteristics of repeatable error, the output frequency

will be stable. The VLC might be regarded as an internal model of the repeatable error. Then the output-signal error contains only the wow-flutter spectrum of the motor. To make the discussion simple, consider the following example:

- Number of sectors on an optical disk = 1000 sectors.
- Motor revolution cycle = 60 Hz.
- PLL output frequency = 60 MHz.

In this case, the nominal counter value of the VLC is obtained as

$$\frac{60\ 000\ 000}{1000\ \times\ 60} = 1000. \tag{1}$$

If there is no sensor error, 1000 for every sector is the best value to stabilize the frequency of the PLL output. The values are changed in all other cases. For example, when the sector length is too long, the counter value is set larger; if sector length is too short, it is set smaller. The sector number is addressed by an SRC (sector-ring counter), which counts the sector pulses from the VLC. Therefore, the counter value can be changed at every sector. The WFG (window-frame generator) generates a reference window frame from the crystal oscillator. The output frequency is the same as the averaged value of the PLL input frequency. The FCC (frame-clock counter) counts the number of PLL output pulses during each reference window frame. The MPU calculates and stores the VLC counter value from the FCC output data. The sum of all data must be $1000 \times 1000 = 1000000$ to keep the PLL output frequency at 60 MHz. The VLC counter value converges after several iterations of the above tuning sequence, and the repeatable error is then eliminated on the PLL output.

Post-writer

• Configuration

There are two modes in the post-writer stage. In the calibration mode, the disk RRO components are measured in advance of the proper pattern-writing mode. The actuator is exercised and parked at the outer crash stop by a constant VCM (voice-coil motor) current. Then the RRO components are measured by reading the master servo pattern with the file's own head at the crash stop position, as shown in Figure 10. The detected data are stored in the RAM (random-access memory) table. The actuator position is controlled by a sector servo system that refers to both the master pattern and the table. The head position can then be controlled to follow the proper tracks, which are concentric with the disk spindle.

A proper sector servo pattern is written on each disk surface (including the master disk itself) by

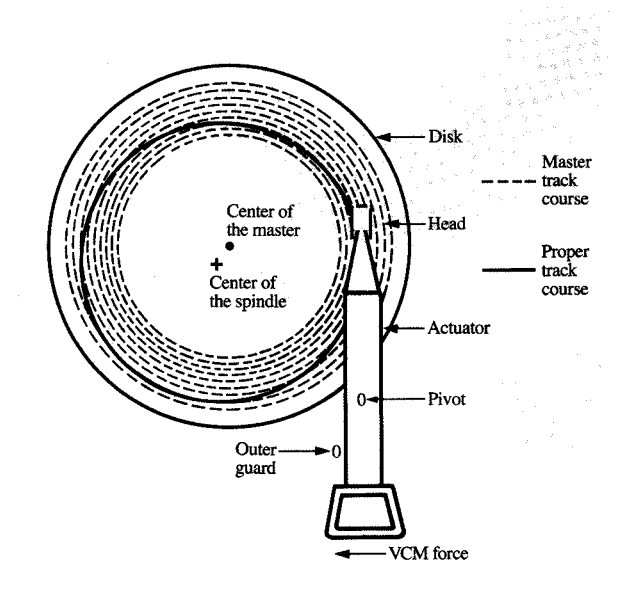


Figure 10
RRO measurement at post stage.

circumferentially skipping every second replication of the master pattern (see Figure 5). In the case of a dedicated servo product, the continuous pattern is written through a servo-dedicated channel onto each dedicated surface which is different from the master surface (for example, the opposite side of the master surface.)

• Actuator control

To realize table-lookup RRO compensation, digital actuator control is necessary. However, there are mechanical resonance problems caused by aliasing when digital signal processing is used. The post-writer uses a product-file head/actuator whose resonant frequency depends on the file mechanism and is not high enough to be ignored. Conventionally, electrical notch filters are used to reduce the problem, as shown in **Figure 11**. However, this method is not robust enough to overcome the variance in resonant frequency [4, 5].

In ESPER-2, an analog LPF (low-pass filter) is applied between the DAC and the power amplifier to reduce the high-frequency spectrum of the VCM current (Figure 12, part 1). The pole of the first-order LPF is placed at around 1/10 of the sampling period. Loss in the servo band is regained by a digital compensator, as shown in part 2 of Figure 12.

The above idea is realized by designing an optimal servo controller using an accurate discrete model. The model describes not only the dynamics of the VCM-actuator

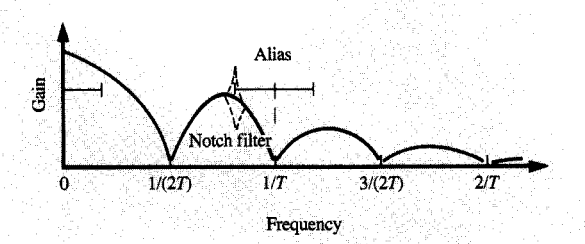
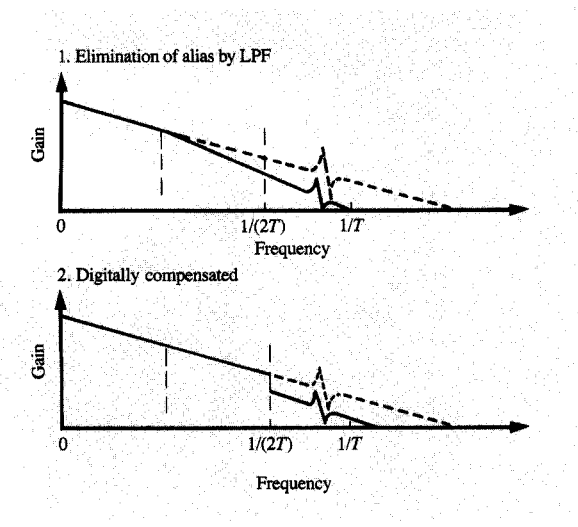


Figure 1

Frequency response of actuator with notch filter.



Frequency response of actuator with LPF and digital compensator

system but also an LPF for digital sampling. The loss due to the LPF in the servo bandwidth is naturally regained by the servo controller. Given the assumption of linear continuous modeling, the LPF-actuator system transfer function is given by Equation (2),

$$\frac{y(s)}{u(s)} = \frac{bc}{s^2(s+a)},\tag{2}$$

where a is the pole of the LPF, b is the input gain, and c is the output gain. (Actually, there are additional resonant modes, but their frequencies are higher than the Nyquist frequency and they are negligible here.)

Equation (3) is the continuous-state equation; the output equation is Equation (4):

$$\dot{\mathbf{x}}(t) = \mathbf{A}_{c}\mathbf{x}(t) + \mathbf{B}_{c}u(t), \tag{3}$$

$$y(t) = \mathbf{C}\mathbf{x}(t),\tag{4}$$

where u(t) is the input (DAC output) at time t. If x is defined as the head position, the state vector x is

$$\mathbf{x}(t) = \left[\mathbf{x}(t), \dot{\mathbf{x}}(t), \ddot{\mathbf{x}}(t) \right]^{T}, \tag{5}$$

and the system matrices A_c , B_c , and C are as follows:

$$\mathbf{A}_{c} = \begin{bmatrix} 0 & 1 & 0 \\ 0 & 0 & 1 \\ 0 & 0 & -a \end{bmatrix},\tag{6}$$

$$\mathbf{B}_{c} = \begin{bmatrix} 0 & 0 & b \end{bmatrix}^{T}, \tag{7}$$

$$\mathbf{C} = [c \ 0 \ 0]. \tag{8}$$

The actuator angle, which is detected as the head position signal, is sampled over period T. Given the holder characteristics of the DAC output and a computational delay τ , the discrete-state equation is obtained as Equations (9) and (10) (see also **Figure 13**):

$$\mathbf{x}(i+1) = \mathbf{A}\mathbf{x}(i) + \mathbf{B}_{i}u(i) + \mathbf{B}_{j}u(i-1), \tag{9}$$

$$y(i) = \mathbf{C}\mathbf{x}(i),\tag{10}$$

where the matrix A and the vectors B_1 and B_2 are as follows:

$$\mathbf{A} = \exp\left(\mathbf{A}_{c}T\right),\tag{11}$$

$$\mathbf{B}_{1} = \int_{0}^{T-\tau} \exp\left(\mathbf{A}_{c}t\right) dt \; \mathbf{B}_{c} , \qquad (12)$$

$$\mathbf{B}_{2} = \int_{T-c}^{T} \exp\left(\mathbf{A}_{c}t\right) dt \; \mathbf{B}_{c} \; . \tag{13}$$

The discrete transition matrix A is given by

$$\mathbf{A} = \mathbf{I} + \mathbf{A}_c T + \frac{(\mathbf{A}_c T)^2}{2!} + \frac{(\mathbf{A}_c T)^3}{3!} + \cdots$$
 (14)

When Equation (14) is analytically solved [6], Equation (15) results:

$$\mathbf{A} = \begin{bmatrix} 1 & T - (1 - aT - \exp^{-aT})/a^2 \\ 0 & 1 & (1 - \exp^{-aT})/a \\ 0 & 0 & \exp^{-aT} \end{bmatrix}.$$
 (15)

Then the discrete input vectors \mathbf{B}_1 and \mathbf{B}_2 are obtained:

$$\mathbf{B}_{1} = [b_{11} \ b_{21} \ b_{31}]^{T}, \tag{16}$$

$$\mathbf{B}_{2} = [b_{1}, b_{2}, b_{32}]^{T}, \tag{17}$$

where the elements are

$$b_{11} = b \frac{1 - a(T - \tau) + \frac{a^2(T - \tau)^2}{2} - \exp^{-a(T - \tau)}}{a^3},$$
 (18)

H. ONO

$$b_{21} = -b \frac{1 - a(T - \tau) - \exp^{-a(T - \tau)}}{a^2}, \tag{19}$$

$$b_{31} = b \, \frac{1 - \exp^{-a(T-\tau)}}{a},\tag{20}$$

$$a\tau - \frac{a^2}{2}\tau(2T - \tau) + \exp^{-aT} - \exp^{-a(T - \tau)}$$

$$b_{12} = -b \frac{a^2}{a^3}, \quad (21)$$

$$b_{22} = b \frac{a\tau + \exp^{-aT} - \exp^{-a(T-\tau)}}{a^2},$$
 (22)

$$b_{32} = -b \frac{\exp^{-aT} - \exp^{-a(T-\tau)}}{a}.$$
 (23)

Next, Equation (9) is extended to the standard format of the state equation, with a digital integrator term v which represents the internal model of the servo system. By defining the extended state vector $\mathbf{x}_d(i)$ as

$$\mathbf{x}_{d}(i) = [x(i), \dot{x}(i), \ddot{x}(i), u(i-1), v(i)]^{T},$$
(24)

the extended state equation is obtained:

$$\mathbf{x}_{d}(i+1) = \mathbf{A}_{d}\mathbf{x}_{d}(i) + \mathbf{B}_{d}u(i), \tag{25}$$

where the matrix \mathbf{A}_d and vector \mathbf{B}_d are

$$\mathbf{A}_{d} = \begin{bmatrix} \mathbf{A} & \mathbf{B}_{2} & \mathbf{0}^{3\times 1} \\ \mathbf{0}^{1\times 3} & 0 & 0 \\ \mathbf{C} & 0 & 1 \end{bmatrix}, \tag{26}$$

$$\mathbf{B}_{d} = \left[\mathbf{B}_{1}^{T}, 1, 0\right]^{T}. \tag{27}$$

The optimal servo controller is obtained by the following LQ method. The cost function J is determined by selecting the weighting matrixes $\mathbf{Q} \in R^{5\times 5}$ and $\mathbf{R} \in R^{1\times 1}$ such that

$$J = \frac{1}{2} \sum_{i=0}^{\infty} \left[\mathbf{x}_d(i)^T \mathbf{Q} \mathbf{x}_d(i) + u(i)^T \mathbf{R} u(i) \right].$$
 (28)

The feedback gain **F** is obtained by solving the following Riccati equations:

$$\mathbf{P}(i+1) = \mathbf{Q} + \mathbf{A}_d^T \mathbf{P}(i) \mathbf{A}_d - \mathbf{A}_d^T \mathbf{P}(i) \mathbf{B}_d \mathbf{F}(i), \tag{29}$$

$$\mathbf{F}(i) = \left[\mathbf{R} + \mathbf{B}_d^T \mathbf{P}(i) \mathbf{B}_d\right]^{-1} \mathbf{B}_d^T \mathbf{P}(i) \mathbf{A}_d. \tag{30}$$

Then the optimal feedback system input is

$$u(i) = -\mathbf{F}(\infty)\mathbf{x}(i). \tag{31}$$

To estimate the state vector \mathbf{x} , a Kalman filter is used. The design algorithm is similar to the controller case above. Figure 14 shows open-loop and closed-loop Bode plots simulating the system of actuator and controller, where the sampling frequency is 4680 Hz and the computing delay time is 100 μ s. About 30 degrees of phase margin and -6 dB of gain margin are obtained with 300 Hz

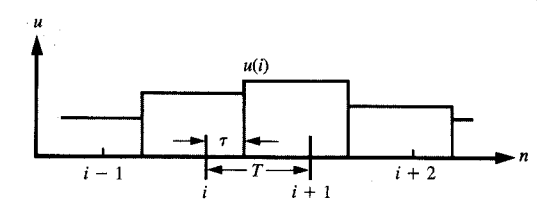
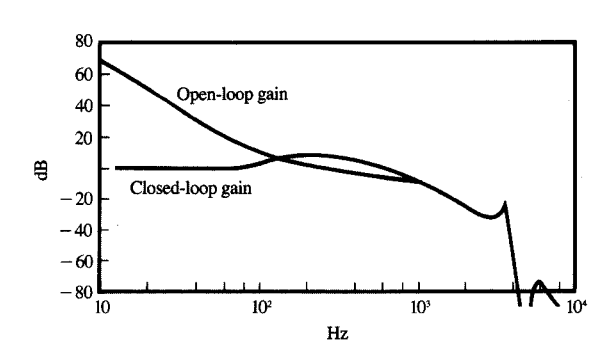


Figure 13

DAC output with computational delay



Open- and closed-loop frequency response of the post-writer actuator control system.

of open-loop bandwidth. The closed-loop curve shows a big loss in high-frequency gain, especially for the range beyond the Nyquist frequency (2340 Hz). Then the mechanical resonance mode at 3500 Hz is attenuated by the analog LPF.

• Read/write operation

Like the pre-writer, the post-writer needs a stable and synchronous system clock for the read/write operation. The VLC-PLL can provide high-quality clock synchronization to the readback sector signal of the master pattern instead of the optical sensor signal. Then the influence of the disk RRO components is canceled by the table-lookup method. The table is generated in the calibration mode. Read/write timing for the proper sectors is controlled by counting the system clock to skip the master sector.

Table 1 Process speed and cost comparison. Assumptions: four disks; 2500 tracks per surface; format, regular quad-burst PES; PES check function included; setup time, 1 min total.

Check item	Conventional writer	ESPER-2		
		Pre	Post	Through
Operation time (min) Cost/file (normalized)	15 1	0.5 1/5	15 1/5	

Performance study

Accuracy

With two-stage writing, all RRO components are electrically canceled. NRRO components are analyzed as follows (all data are specified to show less than 3σ of variance).

Pre-writer

• NRRO of air spindle $\delta_1 = \pm 0.025 \ \mu m$ • Head-positioning accuracy $\delta_1 = \pm 0.05 \ \mu m$

Post-writer

• Head-positioning accuracy $\delta_3 = \pm 0.2 \, \mu \text{m}$

The total NRRO is given by Equation (32):

$$Total_NRRO = \pm \sqrt{\delta_1^2 + \delta_2^2 + \delta_3^2} = \pm 0.208 \ \mu \text{m}.$$
 (32)

Conventional writer accuracy is $\pm 0.27~\mu m$ for the same product-spindle NRRO. Thus, ESPER-2 has better head-positioning accuracy.

Sector-partitioning accuracy is specified as $\pm 0.1~\mu s$. This value is small enough to meet the file requirement, which is $\pm 2~\mu s$, and nonrepeatable jitter can be controlled to within $\pm 10~ns$.

Process speed and cost

The process speed and cost comparison results are shown in **Table 1**. The pre-writer processes ten disks at once. In addition, the writing time is independent of the number of disks mounted in a file. Therefore, the pre-writer operation time is approximately 1/20 of that for the conventional method. The pre-writer is somewhat expensive because of the fine actuator mechanism, but total pre-writer cost is nevertheless only about 1/5 of conventional writer cost. Post-writer process time is similar to that of a conventional writer, so its cost depends only on the price of the equipment. Thus, the grand total is estimated at 2/5 of the cost of a conventional writer.

Conclusions

This paper describes the architecture of the ESPER-2 servo writer. The theoretical study and simulation have been completed and a prototype system has been developed to meet 3.5-inch, 1600-TPI HDD specifications for trial writing. It works very well, and test results show approximately 30 percent better accuracy than that of a conventional writer. The largest contribution to this improvement is pre-writer accuracy. Post-writer accuracy is very independent on magnetic recording noise, which is peculiar to each HDD and disturbs the servo control of master track following. However, magnetic characteristics will gradually be improved, and post-writer accuracy will improve correspondingly in future hard files. Other advantages of ESPER-2 (low cost, reduction of cleanroom requirements) are also confirmed by the prototype. However, some disk-handling machines should still be installed to carry and set master disks in manufacturing.

Acknowledgments

We thank T. Takizawa of storage M & D IBM Fujisawa and his team for giving us product information. We acknowledge M. Fujisaki and T. Murooka and his team of SONY/Tektronix Corporation, and S. Tsujikado and K. Ikarugi of IBM Fujisawa MTD for their assistance on the prototype development. We also acknowledge our indebtedness to T. Hisano of IBM Fujisawa and to M. Sri-Jayantha and his team of IBM Yorktown, and express appreciation to M. Cook, H. Watabe, K. Noda, and K. Kaneko of IBM Fujisawa MTD for encouragement. Finally, we would like especially to express our appreciation to H. H. Ottesen of IBM Rochester CSL for a great deal of technical advice.

References

- C. Lee, "Servowriters: A Critical Tool in Hard Disk Manufacturing," Solid State Technol. 34, No. 5, 207-211 (1991).
- H. Ono and K. Noda, "Architecture of New Servo Writer ESPER," Proceedings of the 1989 IEICE, Institute of Electronics, Information, and Communication Engineers, Japan.
- 3. Laser Rotary Encoder X-1 Specification, Canon Inc., Minato-ku, Tokyo, Japan.
- G. F. Franklin, J. D. Powell, and M. L. Workman, *Digital Control of Dynamic Systems*, 2nd ed., Addison-Wesley Publishing Co., Reading, MA, 1990.
- C. D. Mee and E. D. Daniel, Magnetic Recording, McGraw-Hill Book Co., Inc., New York, 1988.
- S. Wolfram, Mathematica, A System for Doing Mathematics by Computer, Addison-Wesley Publishing Co., Reading, MA, 1991.

Received October 24, 1991; accepted for publication November 11, 1992 Hiroyuki Ono IBM Japan Display Technology Laboratory, LAB-R51, 1623-14, Shimotsuruma, Yamato-shi, Kanagawa-ken 242, Japan (JL04413 at YMTVM8). Mr. Ono is currently a staff engineer in manufacturing technology at the IBM Japan Yamato Laboratory, where he is working on the development of liquid crystal display cells. He received a B.S. in communication engineering from the University of Electro-Communications, Chofu, Tokyo, in 1983, and joined IBM Japan in that year at the Fujisawa facility for an assignment in test engineering. He was later assigned to manufacturing technology development at Fujisawa, where he performed the work reported in this paper. Mr. Ono's professional interests include signal processing, digital control, and process automation. He is a member of the Society of Instrument and Control Engineers and the Institute of Electronics, Information, and Communication Engineers, both of Japan. He received the IBM Outstanding Technical Achievement Award in 1990 for his work on ESPER.